What is Minimal Model of ^{3}He Adsorbed on Graphite?
–Importance of Density Fluctuations in 4/7 Registered Solid–

Shinji Watanabe and Masatoshi Imada

Department of Applied Physics, University of Tokyo, Hongo 7-3-1, Bunkyo-ku, Tokyo, 113-8656,

Japan

We show theoretically that the second layer of ^{3}He adsorbed on graphite and solidified at 4/7 of the first-layer density is close to the fluid-solid boundary with substantial density fluctuations on the third layer. The solid shows a translational symmetry breaking as in charge-ordered insulators of electronic systems. We construct a minimal model beyond the multiple-exchange Heisenberg model. An unexpectedly large magnetic field required for the measured saturation of magnetization is well explained by the density fluctuations. The emergence of quantum spin liquid is understood from the same mechanism as in the Hubbard model and in κ-$(ET)_2Cu_2(CN)_3$ near the Mott transitions.

KEYWORDS: quantum spin liquid, ^{3}He, 4/7 phase, saturation field, Mott insulator, charge order

^{3}He layers adsorbed on graphite substrate is a unique two-dimensional correlated Fermion system and have continuously offered fundamental issues in condensed matter. In particular, adsorption of ^{3}He to the 2nd layer under the corrugation potential of the 1st-layer solid shows a variety of phenomena ranging from a correlated Fermi liquid to a solidification at the commensurate density of 4/7 relative to the 1st layer.[1] The solid phase bahaves as a quantum spin liquid (QSL),[2,3] the nature of which is a long-standing theoretical challenge.[4]

This solidified ^{3}He monolayer has widely been studied by the Heisenberg model with multiple spin exchange (MSE).[5,6] However, exact diagonalization studies on realistic MSE models suggest an opening of spin excitation gap[7] in contrast to the gapless nature of QSL revealed by specific heat[2,8] and magnetic susceptibility measured down to 10 μK.[3,6] Furthermore, the MSE model predicts that the magnetization m saturates above the field $h_{\rm sat} \sim 7$ Tesla,[7,9] whereas a recent experiment[10] up to 10 Tesla indicates the saturation at much higher $h_{\rm sat}$.

A gapless QSL was reported in numerical studies as the ground state of the two-dimensional Hubbard model with geometrical frustration effect near the Mott transition[11–13] supplemented by a report showing numerically the absence of various symmetry breakings.[14] It supports the realization of a genuine Mott insulating state without any translational symmetry breaking as initially proposed by Anderson.[4] This series of studies is indeed relevant and provides a realistic model for a subsequently discovered gapless spin liquid in κ-$(ET)_2Cu_2(CN)_3$. Although a charge gap exists in Mott insulating states, density fluctuations allowing doubly

occupied sites in the Hubbard model near the Mott transition is crucial for the stabilization of the QSL.

However, when we consider the hard core of the interatomic interaction between ^{3}He atoms, the Hubbard model with a moderate onsite interaction U near the Mott transition with a crucial role of density fluctuations looks unrealistic as a model of ^{3}He monolayer.

In this letter, we show that the 4/7-density solid is actually located in the vicinity of the fluid-solid boundary implying essentially the same character as the QSL found in the Hubbard model with substantial density fluctuations, contrary to the conventional picture. More precisely, the density fluctuation in the solid between the 2nd and 3rd layers accompanied by a translational symmetry breaking on the 2nd layer solves the puzzles: It causes enhancement of the ratio of h_{sat} to the exchange interaction as is revealed in the recent experiment.[10] Furthermore, it naturally explains why the MSE model is insufficient to describe the 4/7 phase of ^{3}He.

In the 4/7 phase, the 3/4 of ^{3}He atoms on the 2nd layer occupy points just above mid points of the edges of triangles formed by the 1st-layer atoms whereas the 1/4 occupy points just above the 1st-layer atoms in a regular fashion as shown in Fig. 1(a). Here, open circles represent the atoms on the 1st layer and shaded circles represent actual locations of ^{3}He atoms on the 2nd layer when solidified. If ^{3}He atoms are adsorbed on the 1st layer, it forms a triangular lattice with the lattice constant $a = 3.1826$ Åat the saturation density $\rho_1 = 0.114$ atom/Å^2.[1]

The location of the 2nd-layer atoms is in principle determined as stable points in continuum space. In the present treatment, we simplify the continuum by discretizing it with as much as large number of lattice points kept as candidates of the stable points in the solid. To illustrate the discretization, we cut out from Fig. 1(a) a parallelogram whose corners are just above 4 atoms on the 1st layer as in Fig. 1(b). Possible stable locations of ^{3}He atoms on the 2nd layer are (1) the points just above the mid points of the 1st-layer atoms, (2) the centers of the regular triangles and (3) the points just above the 1st-layer atoms. Therefore, we employ totally 6 points as the discretized lattice points in a parallelogram as circles in Fig. 1(b). Since a unit cell in Fig. 1(a) contains 7 parallelograms, it contains 42 lattice points in total as illustrated as circles in Fig. 1(c). Now the 4/7 solid phase is regarded as a regular alignment of 4 atoms on 42 available lattice points in the unit cell shown in Fig. 1(c).

We employ the Lennard-Jones potential

$$V_{\mathrm{LJ}}(r) = 4\epsilon \left[(\sigma/r)^{12} - (\sigma/r)^6 \right], \tag{1}$$

for the inter-helium interactionwhere $\epsilon = 10.2$ K and $\sigma = 2.56$ Å.[15] More refined Aziz potential is expected to give similar results under this discretization. In the inset of Fig. 2, $V_{\mathrm{LJ}}(r)$ vs. r in the unit of a is shown by the bold solid curve. The interaction term of the lattice model is
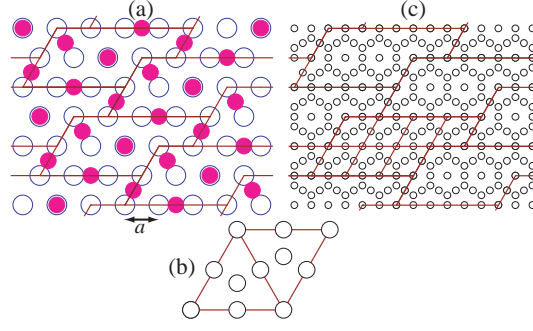
Fig. 1. (Color online) (a) Lattice structure of the 4/7 phase of ^{3}He. Both 1st-layer atoms (open circles) and 2nd-layer atoms (shaded circles) form triangular lattices in the solid phase. The area enclosed by the solid line represents the unit cell for the solid of the 2nd-layer atoms (see text). The lattice constant of the 1st layer is a. (b) Possible stable location of the 2nd-layer atoms are shown by circles on top of a $a \times a$ parallelogram constructed from the 4 neighboring 1st-layer atoms. (c) Structure of discretized lattice for the 2nd-layer model. Lattice points are shown by circles.

given by $H_V = \sum_{ij} V_{ij} n_i n_j$ (n_i is a number operator of a Fermion on the i-th site) with V_{ij} taken from the spatial dependence of eq. (1) on the lattice points. In the actual ^{3}He system, the chemical potential of the 3rd layer is estimated to be 16 K higher than the 2nd layer.[16] ^{3}He atoms may fluctuate into the 3rd layer over this chemical potential difference and it is signaled by an increase of the specific heat for $T > 1$ K[8,17,18] as is reflected by the entropy per site larger than $k_B \log 2$. To take account of this density fluctuation, we here mimic the allowed occupation on the 3rd-layer by introducing a simple finite cutoff V_{cutoff} for V_{ij} within the same form of Hamiltonian: When $V_{\mathrm{LJ}}(r_{ij})$ for $r_{ij} \equiv |\mathbf{r}_i - \mathbf{r}_j|$ exceeds V_{cutoff}, we take $V_{ij} = V_{\mathrm{cutoff}}$ and otherwise $V_{ij} = V_{\mathrm{LJ}}(r_{ij})$. This allows taking account qualitative but essential part of possible occupation on the 3rd layer by the atoms overcoming V_{cutoff}. We show the case of $V_{\mathrm{cutoff}} = 16$ K as indicated by an arrow in the inset of Fig. 2. Here, the open circles show $V(r_{ij})$ on the lattice sites in Fig. 1(c) for $r/a \leq 2$.

Our Hamiltonian for the lattice model $H = H_K + H_V$ consists of the kinetic energy $H_K = -\sum_{\langle ij \rangle}(t_{ij} c_i^\dagger c_j + \mathrm{H.C.})$ and H_V. By using the unit-cell index s and the site index l in the unit cell, we have $\mathbf{r}_i = \mathbf{r}_s + \mathbf{r}_l$.

After the Fourier transform, $c_i = c_{s,l} = \sum_{\mathbf{k}} c_{\mathbf{k},l} e^{i\mathbf{k}\cdot\mathbf{r}_s}/\sqrt{N_u}$, the mean-field (MF) approximation with the diagonal order parameter $\langle n_{\mathbf{k},l} \rangle$ leads to $H_V \sim H_V^{\mathrm{MF}}$

$$= \frac{1}{N_u} \sum_{l,m=1}^{42} \sum_{s'} V^{lm}(s') \sum_{\mathbf{k},\mathbf{p}} \left[\langle n_{\mathbf{k},l} \rangle n_{\mathbf{p},m} - \frac{1}{2} \langle n_{\mathbf{k},l} \rangle \langle n_{\mathbf{p},m} \rangle \right],$$

where the inter-atom interaction is expressed as $V_{ij} = V_{st}^{lm} = V^{lm}(s')$ with $\mathbf{r}_{s'} = \mathbf{r}_s - \mathbf{r}_t$. Then, we have the MF Hamiltonian $H_{\mathrm{MF}} = H_K + H_V^{\mathrm{MF}}$. By diagonalizing the 42×42 Hamiltonian
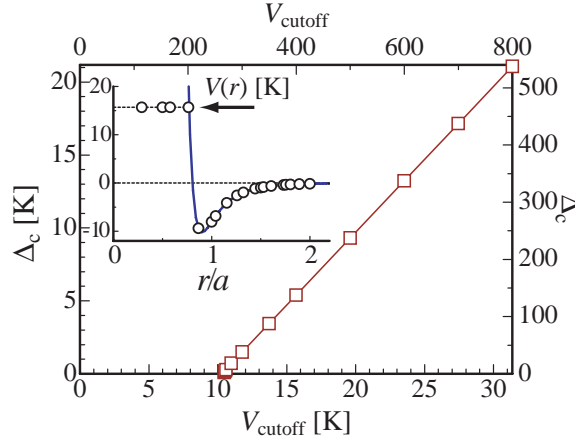
Fig. 2. (Color online) V_{cutoff} dependence of the "charge gap" Δ_{c}. The inset shows the He-He interaction $V(r)$ vs. r (see text).

matrix for each $\mathbf{k}$, we obtain the energy bands $H_{\mathrm{MF}} = \sum_{\mathbf{k}} \sum_{l=1}^{42} E_l(\mathbf{k}) c_{\mathbf{k},l}^{\dagger} c_{\mathbf{k},l}$.

Here we show the results by taking account of the transfers and interactions for $|r_{ij}|/a \leq 2$ as indicated by the open circles in Fig. 2. Then, V_{ij} and t_{ij} for the ij pairs up to the shortest-19th r_{ij} are retained. For the kinetic energy, several choices of t_{ij} are examined and here we show the result for $t_{ij} = t_0/r_{ij}^2$, assuming that it is proportional to $\hbar/(2mr_{ij}^2)$. We note that the kinetic energy per atom for the 4/7 phase is estimated as 20 K by the path-integral Monte Calro (PIMC) simulation.[19] Hence, we evaluate t_0 by imposing the condition, $\sum_{\langle ij \rangle} t_0/r_{ij}^2 \langle c_i^{\dagger} c_j + \mathrm{H.C.} \rangle/(4N_{\mathrm{u}}) = 20$ K. We thus obtain $t_0 = 0.0392$ K, which is taken as the energy unit. The values of ϵ and σ in eq. (1) are given by $\epsilon/t_0 = 260.14$ and $\sigma/a = 0.8045$, respectively. If t_0 is determined so as to reproduce the total kinetic energy of the PIMC result, the main result measured in the unit of K shown below is quite insensitive to the choice of t_{ij}.[20]

By solving the MF equations for H_{MF}, we have the solution of the $\sqrt{7} \times \sqrt{7}$ commensurate structure shown in Fig. 1(a) for $V_{\mathrm{cutoff}} \geq 267t_0 \equiv V_{\mathrm{cutoff}}^{\mathrm{c}}$. The "charge gap" opens for $V_{\mathrm{cutoff}} \geq V_{\mathrm{cutoff}}^{\mathrm{c}}$, as shown in Fig. 2. Here, the "charge gap" is defined by $\Delta_{\mathrm{c}} = E_5^{\mathrm{min}}(\mathbf{k})\text{-}E_4^{\mathrm{max}}(\mathbf{k})$, where $E_l^{\alpha}(\mathbf{k})$ denotes the minimum or maximum value of the l-th band from the lowest. The left (right) and bottom (top) axes represent Δ_{c} and V_{cutoff} in the unit of K (t_0), respectively. From the specific heat data, Δ_{c} is estimated to be ~ 1 K. This leads to $V_{\mathrm{cutoff}}/t_0 \sim 300$ (namely, 12 K), which is consistent with the chemical potential difference of the 3rd layer ~ 16 K.[16] Since $V_{\mathrm{cutoff}}/V_{\mathrm{cutoff}}^{\mathrm{c}} \sim 1.1$, the 4/7 phase is located close to the fluid-solid boundary. The effect of 3 K higher potential on top of the 1st layer ^{3}He than other lattice points of the 2nd layer[21] merely shifts the $\Delta_{\mathrm{c}}\text{-}V_{\mathrm{cutoff}}$ line toward larger V_{cutoff}: $V_{\mathrm{cutoff}}^{\mathrm{c}}$ is changed from ~ 11 K to ~ 14 K and hence the above conclusion does not change.

To further understand the nature of the solid near the fluid-solid boundary, we next

consider a minimal model $\tilde{H} = \tilde{H}_K + \tilde{H}_U + \tilde{H}_V$ with $\tilde{H}_K = -\sum_\sigma \sum_{\langle ij \rangle} \left(t_{ij} c_{i\sigma}^\dagger c_{j\sigma} + \text{H.C.} \right)$, $\tilde{H}_U = U \sum_i n_{i\uparrow} n_{i\downarrow}$ and $\tilde{H}_V = \sum_{\langle ij \rangle} V_{ij} \sum_{\sigma,\sigma'} n_{i\sigma} n_{j\sigma'}$, where $n_{i\sigma} = c_{i\sigma}^\dagger c_{i\sigma}$ and $\langle ij \rangle$ denotes the pair of the sites. To simulate the quantum phase transition between fluid and commensurate solid, we consider a triangular lattice with $N = 12$ sites with $N_e = 4$ Fermions (see inset of Fig. 4). When the nearest neighbor repulsion $V \equiv V_{ij}$ is large in comparison with the transfer, a commensurate solid is expected to be realized. To make accurate estimates of physical quantities we employ the exact diagonalization. Here the transfer integrals with the αth nearest-neighbor t_α for $\alpha \leq 3$ and the nearest-neighbor repulsion V are retained. We take $t_1 = t_2 = t_3 = 1$ and $U = V$ to express the large kinetic energy and the effect of V_{cutoff} for ^{3}He. Figure 3 shows the "charge gap". Here, we calculate the ground-state energy by introducing the phase factor for the transfer integral: $t_{ij} = \tilde{t}_{ij} \exp[i\vec{\phi} \cdot (\mathbf{r}_i - \mathbf{r}_j)]$, where $\vec{\phi} = \phi_1 \mathbf{b}_1 + \phi_2 \mathbf{b}_2$ with $\mathbf{b}_i$ being a reciprocal lattice vector which satisfies $\mathbf{b}_i \cdot \mathbf{a}_j = \delta_{ij}$. To reduce the finite-size effects, the "charge gap" is defined by $\Delta_c \equiv \max\{\mu_{\min}^+ - \mu_{\max}^-, 0\}$, where $\mu_{\min}^+ = \min_\phi [E(N_e + 2) - E(N_e)]/2$ and $\mu_{\max}^- = \max_\phi [E(N_e) - E(N_e - 2)]/2$ with E being the ground-state energy.[22] We take $\phi_\xi = \gamma \pi/8$ with $\xi = x, y$ and the integer γ running from 0 to 8, i.e., totally 81 mesh points for $N = 12$ and $N = 18$ at the filling $n = N_e/N = 1/3$. The results show little system-size dependence indicating the metal-insulator transition at $V = V_c \sim 10$ in the bulk limit. The inset in Fig. 3 shows the V dependence of the peak value of the equal-time charge and spin correlation functions with the periodic boundary condition (b.c.), $(\phi_x, \phi_y) = (0, 0)$, i.e., $N(\mathbf{q}) = \sum_{i,j} \exp[i\mathbf{q} \cdot (\mathbf{r}_i - \mathbf{r}_j)] (\langle n_i n_j \rangle - \langle n_i \rangle \langle n_j \rangle)/N$ and $S(\mathbf{q}) = \sum_{i,j} \exp[i\mathbf{q} \cdot (\mathbf{r}_i - \mathbf{r}_j)] \langle \mathbf{S}_i \cdot \mathbf{S}_j \rangle/(3N)$. The peak of $N(\mathbf{q})$ at $(q_x, q_y) = (2\pi/3, 2\pi/\sqrt{3})$ increases rapidly around $V = V_c$. The peak in $S(\mathbf{q})$ at $(q_x, q_y) = (\pi/3, \pi/\sqrt{3})$ jumps at a higher $V_s > V_c$ suggesting that a commensurate solid for $V > V_c$ is stabilized without a spin order for $V < V_s$ implying the QSL for $V_c < V < V_s$. The realistic choice of $V/V_c \sim 1.1$ inferred from the MF study is located in this QSL region. We note that the ratio of the 3rd-layer promotion to the 2nd-layer density is estimated to be about 10-20% from the results of double occupancy and the nearest-neighbor $\langle n_i n_j \rangle$ averaged over the 81 phase factors in $N = 12$ for $V/V_c \sim 1.1$.

From the exact diagonalization of $N = 12$ sites with the periodic b.c., the exchange interaction J is estimated from high-temperature part of $\chi(T)$ by the fitting of the high-temperature expansion $\chi(T) = (1 - 3J/T)/T$ on the triangular lattice.[23] By plotting $(1/(\chi T) - 1)T$ vs. T as in Fig. 4, we estimate J from the flat part indicated by the arrows. The system-size dependence of J is quite small as known in the Hubbard chain,[24] where $\chi(T)$ at high T is determined by the local process. Figure 5 (open circle) shows J for each V obtained in this way.

The magnetization is calculated by adding the Zeeman term to $\tilde{H}$: $\tilde{H} - h \sum_i S_i^z$. We define the saturation field h_{sat} at which the total magnetization $m = \sum_i \langle S_i^z \rangle/N$ reaches its saturation value, $m_{\text{sat}} = n/2$. Figure 5 shows h_{sat} for the $N = 18$ sites (open triangle) under the periodic
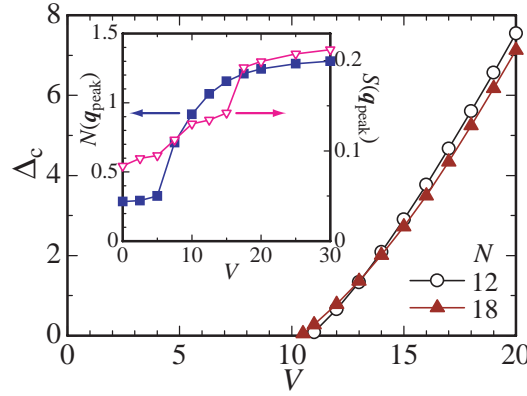
Fig. 3.   (Color online) V dependence of "charge gap" on $N = 12$ (open circle) and $N = 18$ (filled triangle) triangular lattices for $t_1 = t_2 = t_3 = 1$ and $V = U$ at $n = 1/3$. The inset shows V dependence of the peak value of $N(\mathbf{q})$ (filled square) and $S(\mathbf{q})$ (open triangle) for $N = 12$ under periodic b.c.
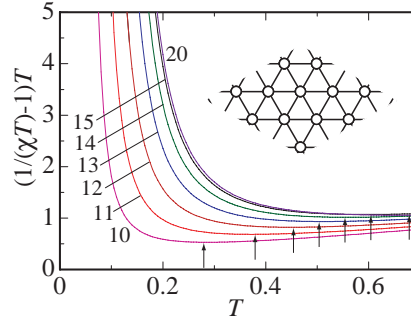

Fig. 4.   (Color online) Temperature and V dependences of susceptibility on $N = 12$ triangular lattice at $n = 1/3$ for $t_1 = t_2 = t_3 = 1$ and $U = V$. The inset shows a triangular lattice with $N = 12$ sites.

b.c. The present saturation field at $V = U = 0$ for $N = 18$ reproduces the exact bulk limit $h_{\text{sat}} = 18.0$, which is nothing but the width of the n-filled band at $h = 0$. This reproduction together with slightly smaller h_{sat} for $N = 12$ (see the inset of Fig. 5) suggests that h_{sat} in Fig. 5 is close to the bulk-limit. This is one of our central results: h_{sat} and hence h_{sat}/J as well largely increase in the commensurate solid near the solid-fluid boundary, $V = V_{\text{c}}$. From Fig. 5, we see that 10 Tesla shown as thin lines is still below the saturation magnetic field for a realistic choice of $V = 11.2$ in agreement with the recent experiment.[10]

Although the enhancement of h_{sat}/J also appears at $t_2 = t_3 = 0$ (not shown), the enhancement is more prominent when t_2 is switched on. This is understood by the perturbation from the large $V(= U)$ limit. When $t_2 = t_3 = 0$, J appears first in the 4th order as $J_{(4)} = 20t_1^4/(3V^3)$, whereas the 2nd-order term $J_{(2)} = 4t_2^2/V$ and the 3rd-order term
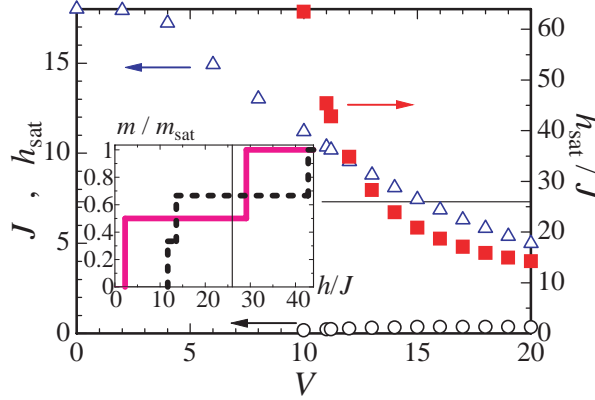
Fig. 5. (Color online) V dependence of exchange interaction J (open circle), saturation field h_{sat} (open triangle) and its ratio h_{sat}/J (filled square) for $t_1 = t_2 = t_3 = 1$ and $V = U$ at $n = 1/3$. The inset shows the magnetization process for $V = 11.2$ in $N = 12$ (solid bold line) and $N = 18$ (broken line) under periodic b.c. The difference between $N = 12$ and 18 may come from different commensurate structures allowed at $m \sim m_{sat}/2$. Thin lines (in the inset as well) represent h/J corresponding to 10 Tesla in the experiment when we employ $J = 0.3$ mK.[25]

$J_{(3)} = -10t_1^2 t_2/V^2$ appear for $t_2 \neq 0$. For $t_2 > 0$, $J_{(3)}$ becomes ferromagnetic (FM), which partially cancels $J_{(4)}$ in $J = J_{(2)} + J_{(3)} + J_{(4)}$. This is similar to the cancellation among anti-ferromagnetic (AF) $J_2 > 0$, FM $-J_3 < 0$ and AF $J_4 > 0$ in the MSE with n-body exchange interactions $(-1)^n J_n$.[5] In short, the enhancement of h_{sat}/J is largely driven by the density fluctuations near the fluid-solid boundary, supplemented by the reduction of AF exchange through partial cancellation by FM MSE.

Let us discuss the significance of the density fluctuations near the fluid-solid boundary in terms of the observed QSL. The QSL in κ-ET$_2$Cu$_2$(CN)$_3$[26] is found in the region of a tiny charge gap,[27] which consistently reproduces the QSL numerically found near the metal-insulator boundary in the Hubbard model on the triangular lattice.[11, 12, 14] The QSL is suppressed when the density fluctuations are suppressed at large U[13] consistently with the absence of the QSL phase reported in the spin-1/2 Heisenberg model on the triangular lattice.[28] They suggest the importance of density fluctuations for the realization of the QSL in the 4/7 phase of ^{3}He.

The density excitations over the energy $\Delta_{\mathrm{c}} \sim 1$ K make a peak in the specific heat $C(T)$ at $T \sim 1$ K in addition to a low-temperature peak around $T = 10^{-1} \sim 1$ mK reflecting the spin excitations, since the exchange interaction is estimated as $J_{(2)} = 4t_{ij}^2/V_{\mathrm{cutoff}} \sim 5 \times 10^{-4}(t_{ij}/t_0)^2$ K. The double-peak structure is indeed found in $C(T)$ for $V \geq 10$ in the $N = 12$ cluster study (not shown) as is observed in ^{3}He.[2, 8]

The fluid-solid transition occurs at a very large $V_{\mathrm{cutoff}}/t_0 \sim 300$ as seen in Fig. 2, which reflects the general tendency that the commensurate solid phase dramatically shrinks when

the period of the density order becomes long.[29] This explains why the fluid-solid boundary is located near such a large chemical potential difference of the 3rd layer.

In summary, we have shown that the minimal model for ^{3}He adsorbed on the graphite should consider the density fluctuation to the upper layers. In particular, the properties of the 4/7-solid phase on the 2nd layer are understood only by considering the density fluctuations on the 3rd layer, which makes the real system close to the fluid-solid transition beyond the description by the MSE model. The magnetic field required for the magnetization saturation is largely enhanced in agreement with the experiments. The density fluctuations also serve as a key for stabilizing the QSL. Our study predicts that when the lattice constant of the 1st-layer solid can be changed, the 4/7 solid phase easily changes to fluid. Experimental tests would be highly desired.

Acknowledgment

References

1) V. Elser: Phys. Rev. Lett. **62** (1989) 2405.

2) K. Ishida, M. Morishita, K. Yawata and H. Fukuyama: Phys. Rev. Lett. **79** (1997) 3451.

3) R. Masutomi, Y. Karaki and H. Ishimoto: Phys. Rev. Lett. **92** (2004) 025301.

4) P. Fazekas and P. W. Anderson: Phil. Mag. **30** (1974) 423.

5) M. Roger, C. Bauerle, Yu. M. Munkov, A.-S. Chen and H. Godfrin: Phys. Rev. Lett. **80** (1998) 1308.

6) H. Ikegami, R. Masutomi, K. Obara and H. Ishimoto: Phys. Rev. Lett. **85** (2000) 5146.

7) G. Misguich, B. Bernu, C. Lhuillier and C. Waldmann: Phys. Rev. Lett. **81** (1998) 1098.

8) Y. Matsumoto, D. Tsuji, S. Murakawa, C. Bäuerle, H. Kambara and H. Fukuyama: unpublished.

9) T. Momoi, H. Sakamoto and K. Kubo: Phys. Rev. B **59** (1999) 9491.

10) H. Nema, A. Yamaguchi and H. Ishimoto: unpublished.

11) T. Kashima and M. Imada: J. Phys. Soc. Jpn. **70** (2001) 3052.

12) H. Morita, S. Watanabe and M. Imada: J. Phys. Soc. Jpn. **71** (2002) 2109.

13) T. Mizusaki and M. Imada: Phys. Rev. B **74** (2006) 014421.

14) S. Watanabe: J. Phys. Soc. Jpn. **72** (2003) 2042.

15) J. de Boer and A. Michels: Physica **5** (1938) 945.

16) P. A. Whitlock, G. V. Chester and B. Krishnamachari: Phys. Rev. B **58** (1998) 8704.

17) S. W. Van Sciver and O. E. Vilches: Phys. Rev. B **18** (1978) 285.

18) D. S. Greywall: Phys. Rev. B **41** (1990) 1842.

19) F. F. Abraham, J. Q. Broughton, P. W. Leung and V. Elser: Europhys. Lett. **12** (1990) 107.

20) In case of $t_{ij} = -t_0$ for ij pairs up to the shortest-19th r_{ij}, the result of Δ_c K vs. V_{cutoff} K is nearly the same as Fig. 2.

21) G. Boato, P. Cantini, C. Guidi, R. Tatarek and G. P. Felcher: Phys. Rev. B **20** (1979) 3957.

22) T. Koretsune, Y. Motome and A. Furusaki: J. Phys. Soc. Jpn. **76** (2007) 074719.

23) W. Opechowski: Physica **4** (1937) 181.

24) In the Hubbard chain, the high-temerature part of $\chi(T)$ in a few sites is quite close to the bulk-limit value; H. Shiba and P. A. Pincus: Phys. Rev B **5** (1972) 1966. See also H. Shiba: Prog. Theor. Phys. **48** (1972) 2171.

25) E. Collin, S. Triqueneaux, R. Harakaly, M. Roger, C. Bauerle, Yu.M. Bunkov and H. Godfrin: Phys. Rev. Lett. **86** (2001) 2447.

26) Y. Shimizu, K. Miyagawa, K. Kanoda, M. Masato and G. Saito: Phys. Rev. Lett. **91** (2003) 107001.

27) I. Kezsmarki, Y. Shimizu, G. Mihály, Y. Tokura, K. Kanoda and G. Saito: Phys. Rev. B **74** (2006) 201101R.

28) B. Bernu, P. Leceminant, C. Lhuillier and L. Pierre: Phys. Rev. B **50** (1994) 10048.

29) Y. Noda and M. Imada: Phys. Rev. Lett. **89** (2002) 176803.